Research Article
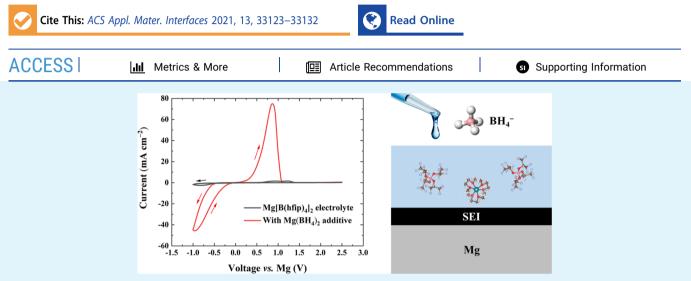
Establishing a Stable Anode−Electrolyte Interface in Mg Batteries by Electrolyte Additive

Zhenyou Li,* Thomas Diemant, Zhen Meng, Yanlei Xiu, Adam Reupert, Liping Wang,
Maximilian Fichtner, and Zhirong Zhao-Karger*

ACCESS | Metrics & More | Article Recommendations | Supporting Information

ABSTRACT: Simple magnesium salts with high electrochemical and chemical stability and adequate ionic conductivity represent a new-generation electrolyte for magnesium (Mg) batteries. Similar to other Mg electrolytes, the simple-salt electrolyte also suffers from high charge-transfer resistance on the Mg surface due to the adsorbed species in the solution. In the current study, we built a model Mg cell system with the $Mg[B(hfip)_4]_2$/DME electrolyte and Chevrel phase Mo_6S_8 cathode, to demonstrate the effect of such anode−electrolyte interfacial properties on the full-cell performance. It was found that the cell required additional activation cycles to achieve its maximal capacity. The activation process is mainly attributed to the conditioning of the anode−electrolyte interface, which could be boosted by introducing an additive amount of $Mg(BH_4)_2$ to the $Mg[B(hfip)_4]_2$/DME electrolyte. Electrochemical and spectroscopic analyses revealed that the $Mg(BH_4)_2$ additive helps to remove the native oxide layer and promotes the formation of a solid electrolyte interphase layer on Mg. As a result, the full cell with the additive-containing electrolyte delivered a stable capacity from the second cycle onward. Further battery tests showed a reversible cycling for 600 cycles and an excellent rate capability, indicating good compatibility of the $Mg(BH_4)_2$ additive. The current study not only provides fundamental insights into the interfacial phenomena in Mg batteries but also highlights the facile tunability of the simple-salt Mg electrolytes.

KEYWORDS: Mg intercalation, noncorrosive electrolyte, electrolyte additive, electrode−electrolyte interfaces, Chevrel phase Mo_6S_8

1. INTRODUCTION

Electrochemical deposits of magnesium (Mg) from a non-aqueous electrolyte solution exhibit a more homogeneous morphology than the monovalent counterparts (Li and Na),[1] allowing the implementation of the metallic Mg anode into the respective battery systems with less safety concern. The resulting rechargeable Mg batteries (RMBs) could theoretically promise solutions for high-energy-density devices in a cost-efficient and sustainable manner.[2] With the development of the first prototype system,[3] the RMB has the potential as an alternative and complementary strategy for the prevalent lithium-ion (Li-ion) technology.[4]

However, transfer of results from the state-of-the-art Li-based technology to the Mg systems is not straightforward, as battery chemistries involving divalent Mg ions are significantly different from the redox reactions that are based on the Li-ion

shuttle.[5] The bivalency and high charge density of Mg^{2+} ions induce a strong tendency to form ion pairs in liquid organic electrolytes,[6,7] providing limited ionic conductivity and generating detrimental interfacial issues.[8] In the electrolyte solution, there are competitions between solvent molecules and anions in coordination with Mg^{2+} ions.[9] Approaches to sufficient cation−anion dissociation include either introducing auxiliary anions with larger association strength (e.g., chloride ions)[10,11] or developing anions that interact weaker with Mg^{2+}
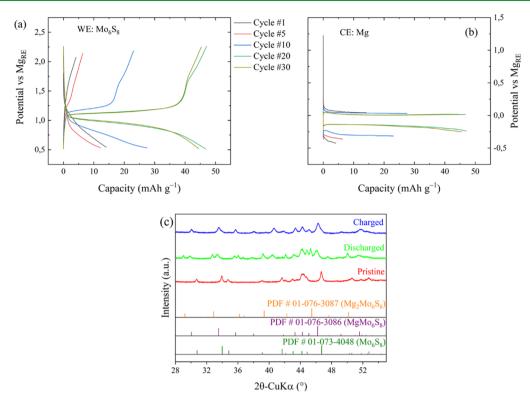
Figure 1. Galvanostatic cycling of a three-electrode cell comprising a Mo_6S_8 working electrode (WE), a Mg reference electrode (RE), and a Mg counter electrode (CE): voltage profiles of the Mo_6S_8 WE (a) and the Mg CE (b). The cell was cycled at 50 mA g^{-1}, with a 0.3 M $Mg[B(hfip)_4]_2$/DME electrolyte. (c) XRD patterns of the electrodes before and after cycling.
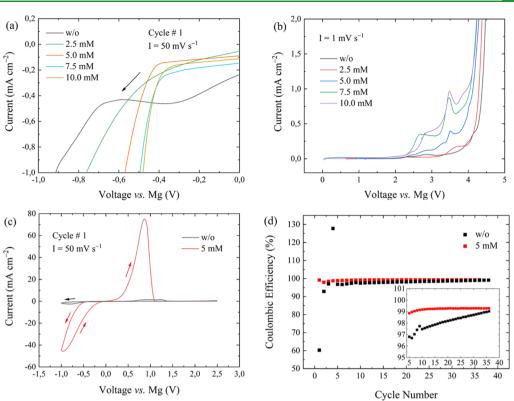
ions than the solvent molecules.[12] The Cl^- ions in the electrolyte were also identified as a multifunctional component and essential for interfacial charge transfer at the anode–electrolyte interfaces.[13,14] However, the corrosive nature of the Cl-based electrolytes limit their practical application. In contrast, the weak coordination concept enables simple ionic solution and exhibits high electrochemical stability and chemical compatibility, which are essential requirements for high-capacity conversion cathodes[15,16] and high-voltage insertion cathodes,[17] therefore representing advanced Mg electrolyte systems.

Despite the abovementioned excellent properties, this type of electrolyte also suffers from a growing anode impedance during open-circuit voltage (OCV), similar to other Mg electrolyte systems.[18] The large impedance was correlated to some electrochemically inactive species in solution that tends to form an adsorption layer on the Mg surface, which hinders the mass transport and results in a huge voltage spike in the initial plating/stripping process. The adsorption layer gradually vanishes upon applying some voltage bias, and the overpotentials quickly drop to a small and stable value with a prolonged cycle in chronopotentiometry studies using symmetric cell configuration.[19] However, overcoming such a huge energy barrier in the case of practical galvanostatic cycling with a limited voltage window may require a long conditioning process, leading to a misevaluation of the cathodes or the cell performance. The unique interfacial issue can be greatly mitigated by replacing the Mg metal anode with the Mg_3Bi_2 alloy, which shows drastic reduction of the anode impedance during OCV.[20] Similar improvement was observed when protecting the pristine Mg surface with a thin MgF_2 layer[21] or an alloy-based interphase,[22] implying that correct control of

the interface is of considerable practical concern in Mg batteries.

In this study, we established a model system to demonstrate the impact of the abovementioned interfacial issue in a full cell, which contains the benchmarking Chevrel phase Mo_6S_8 cathode, magnesium tetrakis(hexafluoroisopropyloxy)borate/ dimethoxyethane ($Mg[B(hfip)_4]_2$/DME) electrolyte and a Mg anode. It was found that reversible Mg de-/intercalation in the $Mg[B(hfip)_4]_2$/DME electrolyte is possible, but the cell requires some activation cycles. Further electrochemical analysis together with spectroscopic study attributed the activation process mainly to the conditioning of the anode–electrolyte interfaces, in addition to some adjustment of the cathode structure. The activation can be alleviated by introducing magnesium borohydride $Mg(BH_4)_2$ as an electrolyte additive, which is beneficial for the removal of the native oxide layer and formation of a solid electrolyte interphase (SEI). By applying the $Mg[B(hfip)_4]_2$ electrolyte with an optimized $Mg(BH_4)_2$ additive concentration, the Mo_6S_8–Mg cell provided an activation-free stable cycling for up to 600 times.

2. RESULTS AND DISCUSSION

2.1. Mg Intercalation into the Mo_6S_8 Cathode from a $Mg[B(hfip)_4]_2$/DME Electrolyte. Mg storage in the Mo_6S_8 cathode seems highly dependent on the chloride-based electrolyte systems, in which the Cl^- ions play decisive roles in the electrode–electrolyte interfaces at both anode and cathode sides.[13,23] So far, the combination of the $Mg[B-(hfip)_4]_2$/DME electrolyte with the insertion cathode was only investigated with either a special cathode design[24] or a novel intercalation chemistry.[25] To validate the feasibility of the

Figure 2. Electrochemical tests of the 0.3 M $Mg[B(hfip)_4]_2$/DME electrolytes with and without the $Mg(BH_4)_2$ additive: (a) initial Mg plating in the first cycle CV scan; (b) LSV of the electrolytes with various additive concentrations; (c) comparison of the first cycle CV with the neat electrolyte and with 5 mM $Mg(BH_4)_2$; (d) Coulombic efficiency of Mg plating/stripping using the neat electrolyte and with 5 mM $Mg(BH_4)_2$. Pt was used as the WE in all the CV and LSV measurements.

model system, Mg intercalation into the Mo_6S_8 cathode was first studied by means of galvanostatic cycling in a three-electrode cell. In order to mimic the two-electrode condition in the later sections, the applied voltage window of the three-electrode cell was set to 0.5−2.5 V versus Mg_{CE}. Figure 1a shows the voltage profiles of the Mo_6S_8 cathode versus Mg_{RE} upon cycling, from which an increase in the capacity in the first 20 cycles was observed. The capacity increase is partially related to an activation process at the cathode side, as indicated by a simultaneous decrease in the charge−discharge overpotentials with more and more prominent voltage plateaus. According to a previous study, diffusion kinetics increases with the increase in Mg content in the Mo_6S_8 lattice.[26] Therefore, a possible reason for the evolution of the charge−discharge curves could be some structural adjustment of the cathode host, which improves further Mg-ion mobility.

Nevertheless, the capacity stabilized at ∼48 mA h g^{-1} after the activation cycles, with a discharge plateau at ∼1.0 V and a voltage hysteresis of ∼0.2 V. To clarify the de-/magnesiation process, electrodes at various states of charge were investigated by X-ray diffraction (XRD). As shown in Figure 1c, the pattern for the discharged sample can be indexed as a mixture of $MgMo_6S_8$ and $Mg_2Mo_6S_8$, while the diffraction of the charged sample results in a pure $MgMo_6S_8$ phase.[27] The XRD data demonstrate that the $Mg[B(hfip)_4]_2$/DME electrolyte supports Mg de-/intercalation in Mo_6S_8, even at a high current of 50 mA g^{-1} (∼0.4 C). The trapping of Mg in the $Mg_xMo_6S_8$ structure may result from a slow diffusion kinetics at a low Mg content ($x < 1$), when Mg ions only occupy the inner rings of the cage.[26] This also explains the respective voltage profile

(Figure 1a), where the higher discharge plateau at ∼1.2 V is missing.

In addition to the cathode contribution, Mg plating/stripping at the anode side could be the main reason for the activation process. As shown in Figure 1b, the Mg stripping process requires initially a very large overpotential of 1.22 V. A similar voltage spike was observed in our previous study with a Mg−Mg symmetric cell using the same electrolyte and could be attributed to electrochemically inactive species adsorbed on the Mg surface that generate a large charge transfer impedance.[19] The voltage spikes still appeared but quickly vanished in the subsequent cycles. In each cycle, the stripping voltage drops to <0.1 V immediately after operating the cell, and the value is further reduced to 0.01 V after 20 cycles. In contrast, the respective plating processes suffer from more pronounced and persistent overpotentials of −0.43 V in the first cycle, which decreases to −0.15 V in the 20th cycle. The large overpotentials for Mg plating in the initial cycles reflect the sluggish charge transfer at the anode side, which could be related to the native oxide layer on fresh Mg foil. This intrinsic layer may impede the de-/magnesiation process at the cathode side and contributes to the overall charge−discharge over-potentials of the full cell (see Figure S1).

2.2. $Mg(BH_4)_2$ as an Additive to the $Mg[B(hfip)_4]_2$/ DME Electrolyte. In order to alleviate the activation process, $Mg(BH_4)_2$ was introduced as an electrolyte additive, with concentrations ranging from 2.5 to 10 mM, in the 0.3 M $Mg[B(hfip)_4]_2$/DME electrolyte. Cyclic voltammetry (CV) experiments of a Mg−Pt cell in Figure 2a showed a significant reduction of the overpotential related to Mg plating in the first cycle with the additive-containing electrolyte. At an onset
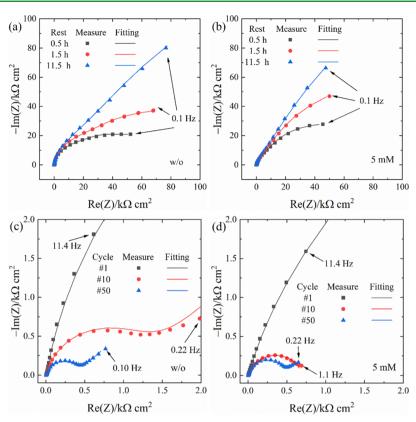
Figure 3. EIS of Mg−Mg symmetric cells after resting in the (a) neat electrolyte or (b) electrolyte with a 5 mM additive and upon cycling in the (c) neat electrolyte or (d) electrolyte with a 5 mM additive.
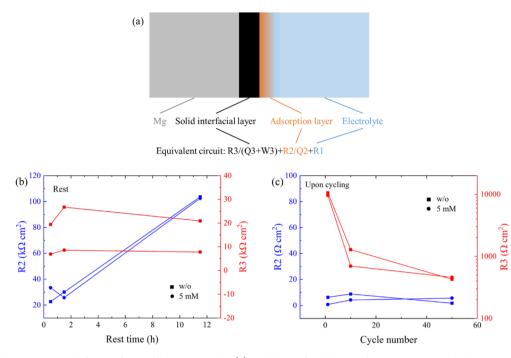
current of −0.6 mA cm^{-2}, a relatively high overpotential of −0.76 V was received for the neat Mg[B(hfip)$_4$]$_2$/DME electrolyte, which is ascribed to the native oxide layer of the Mg foil and the adsorption species at the interfaces that impede Mg-ion mobility.[18,19] With an increasing amount of Mg(BH$_4$)$_2$, the initial plating overpotential gradually decreased to −0.63 V (2.5 mM), −0.52 V (5 mM), and −0.46 V (7.5 mM). A further increase in the Mg(BH$_4$)$_2$ concentration did not change the value any more (−0.45 V for 10 mM).

It should be mentioned that Mg(BH$_4$)$_2$ provides a notably narrow electrochemical window,[28] which limits its application as a bulk electrolyte salt to certain electrode couples. Therefore, the effect of the additive on the electrochemical window of the electrolyte was investigated by linear sweep voltammetry (LSV). In the case of the neat electrolyte (Figure 2b), no obvious current was measured for up to 4.0 V at a scan rate of 1 mV s^{-1}. The oxidative stability of the neat electrolyte is beyond the limit of DME, which might be due to some passivation layers on the surface of the WE which suppress the DME decomposition.[29] In contrast, new oxidation peaks start to form at lower voltages after the addition of Mg(BH$_4$)$_2$ to the electrolyte solution. With an additive concentration of 2.5 mM, a broad peak occurs at around 3.5 V, which originates from the decomposition of the solvent, that is, DME.[12] Emergence of the peak related to DME oxidation might be due to some pitting corrosion of the WE in the presence of BH$_4^-$ (or [B(hfip)$_4$]$^-$ anions). Therefore, the surface of the WE was activated for the decomposition of the solvent. When the Mg(BH$_4$)$_2$ concentration was increased to 5 mM, an additional oxidation peak related to the decomposition of BH$_4^-$ at ∼2.5 V appeared.[28] Further increasing the concentration of Mg(BH$_4$)$_2$

leads to more prominent peaks for the oxidation of BH$_4^-$ and DME, resulting in a reduced electrochemical window.

Considering both the initial overpotentials for Mg plating and the anodic stability, the electrolyte with 5 mM Mg(BH$_4$)$_2$ was selected for further study. Due to the reduced overpotentials, the current response for Mg plating/stripping in the first cycle from the electrolyte with 5 mM Mg(BH$_4$)$_2$ is much more prominent than that from the neat electrolyte, as shown in Figure 2c. Furthermore, the CV curves of the electrolyte with the additive are almost overlapping in the following cycles (see Figure S2), suggesting a reversible and conditioning-free redox process on the Pt electrode. In comparison, Mg plating/stripping from the neat electrolyte suffers from a conditioning process as reported in a previous study.[15] The reversibility of Mg plating/stripping was further examined by the Coulombic efficiency (CE) determined from the CV measurement. As presented in Figure 2d, a stable CE value of ∼99.3% was received for the additive-contained electrolyte, while the CE values for the neat electrolyte showed instability in the first 10 cycles before constantly increasing from 97.5 to 99%.

To clarify the origin of the plating/stripping overpotentials, chronopotentiometry of Mg−Mg symmetric cells was performed, during which electrochemical impedance spectra (EIS) were recorded under both electrochemical static and dynamic conditions. Figure S3 shows the voltage profiles of the symmetric cells with a neat electrolyte (red) and the additive-modified electrolyte [5 mM Mg(BH$_4$)$_2$, green]. With the neat electrolyte, the cell exhibits an initial overpotential of −0.52 V (Figure S3b), which decreases gradually during the plating process. The development of the voltage profile can be explained by a gradual activation of the electrode, possibly due to the removal of the native oxide layer at the counter Mg

Figure 4. Equivalent circuit used for the fitting of the EIS results (a). Solid interfacial layer refers to a native oxide layer on Mg foil under static conditions, while it corresponds to a newly formed SEI layer under dynamic conditions. Development of impedance related to the adsorption layer (R2) and solid passivation layer (R3) during the rest time (b) and upon cycling (c).

electrode and/or building-up of a new interphase. In comparison, the cell with the additive-containing electrolyte shows a plating plateau at −0.20 V with an onset value of −0.35 V, suggesting a kinetically more favorable and more homogeneous plating process. Upon further cycling (see Figure S3a), the plating overpotentials of the cells remained stable at around −0.10 V for both electrolytes, but the additive-containing electrolyte requires less conditioning cycles before reaching the stable state.

The symmetric cells were further tested after letting them rest for 10 h after every 50 cycles, in order to check the influence of the adsorption layer on the continuous switch between "on" and "off" states of a battery. As shown in Figure S4, there is always an overpotential spike noted after every resting period, suggesting a long-term effect. However, due to the conditioning of the Mg surface, the following spikes are only in the range of 0.1−0.2 V, which is much smaller than the first one.

According to previous studies,[18,19] the high impedance in the initial Mg plating process is mainly related to an electrochemically inactive adsorption layer on the electrode surface. When monitoring the process by EIS, a growth of the impedance value during the rest time was observed for both electrolytes (Figure 3a,b). Additionally, we speculate that the native oxide layer on the Mg surface also contributes to the overpotentials. Therefore, a model that considers the above-mentioned processes (see Figure 4a) has been applied to fit the experimental EIS data. In particular, variations of the charge transfer resistances that originated from the adsorption layer (R2) and the solid interfacial layer (R3) are highlighted in Figure 4b. After 0.5 h rest, R2 and R3 contributed almost equally to the total impedance. However, R2 increased rapidly and exceeded 100 kΩ cm^2 after a rest time of 11.5 h, which suggests a growth of the adsorption layer under static conditions. In comparison, the change in R3 over time was

negligible, indicating a good chemical compatibility between both electrolytes and the Mg anode. The addition of the $Mg(BH_4)_2$ additive leads to a significant decrease in R3. This is probably due to a preferential adsorption of the reductive $BH_4^−$ at the interfaces, which is beneficial for removing the thin oxide layer on the fresh Mg anode and thus leading to a lower initial plating overpotential.

Upon cycling, the cell impedance decreased rapidly, as shown in Figure 3c,d. A simultaneous change in voltage hysteresis reveals their correlations (cif. Figure S3). The same equivalent circuit, as shown in Figure 4a, was applied to understand the interfacial charge transfer processes. R2 still represents the impedance induced by the adsorption layer, and R3 shows the impedance of the interphase layer including the remaining oxide layer and the formed SEI. Fitting the EIS data results in a sharp drop of R2 to a neglectable value upon cycling (Figure 4c), which is most probably due to the breakup of the adsorption layer under voltage bias and upon ion shuttling. The impedance related to the adsorption layer did not show a significant difference in both electrolytes, which could indicate that the additive amount of $Mg(BH_4)_2$ would not change the evolution of the adsorption layer. In contrast, there is a gradual change in the impedance related to the solid surface layer (R3) with respect to the cycle number, indicating a conditioning of the intrinsic thin film on the Mg surface. Nevertheless, the cell with the additive-containing electrolyte exhibits fewer conditioning cycles than the one with the neat electrolyte. After 10 cycles, the R3 value in the former case is only half of that in the latter case (696 Ω cm^2 vs 1284 Ω cm^2). Afterward, R3 gets fairly stable in the additive-contained electrolyte. Moreover, after 50 cycles, the R3 values are close to each other for both electrolytes (460 Ω cm^2 vs 427 Ω cm^2). The rapid change in R3 can be attributed to the higher reactivity of $BH_4^−$ and its higher association strength that promote the interfacial charge transfer by facilitating the
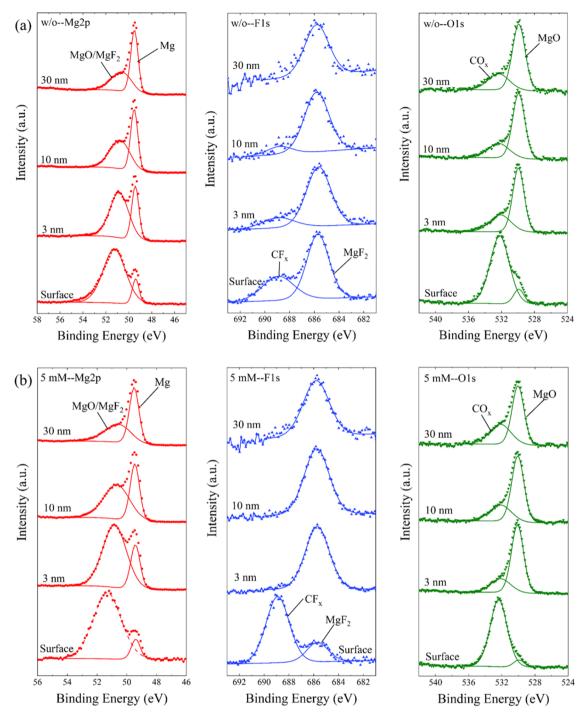
Figure 5. XPS spectra of Mg anodes cycled with the (a) neat electrolyte and (b) additive-containing electrolyte at selected depths.

formation of the SEI.[10] The result demonstrated that a small amount of $Mg(BH_4)_2$ additive is enough to modify the interfacial properties.

To gain more insights into the composition of the interfacial layers on the Mg anodes, X-ray photoelectron spectroscopy (XPS) measurements were carried out. XPS measurements were also collected after Ar^+ ion sputter treatment (for 3, 10, and 30 min, sputter rate ~1 nm min^{-1}) of the samples in order to create a depth profile. Figure S5 compares the development of the elemental concentrations with increasing depth of Mg anodes after initial cycles with the neat electrolyte or additive-containing electrolyte. In both cases, a significant amount of non-Mg metal components was detected on the topmost

surface, indicating the formation of an SEI layer after cycling. Furthermore, the semiquantitative analysis shows a similar trend in both electrolytes with increasing layer depth: a simultaneous reduction of the C, O, F, and B concentrations goes along with an increase in Mg content within the surface region of the Mg anodes. The development of the interfacial compositions suggests that the thickness of the SEI layer was only limited to ~10 nm. Compared to the Mg anode cycled with the neat electrolyte, the one cycled with the additive-containing electrolyte has a lower Mg content but higher content of the other elements at all measured depths, suggesting a slightly thicker SEI.
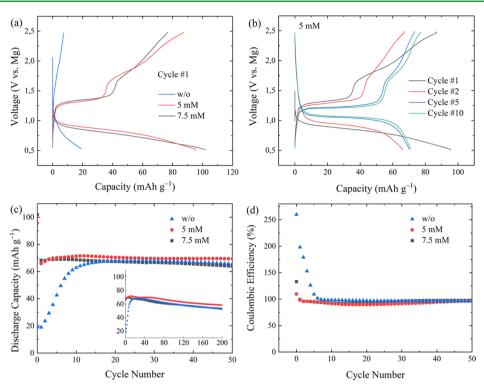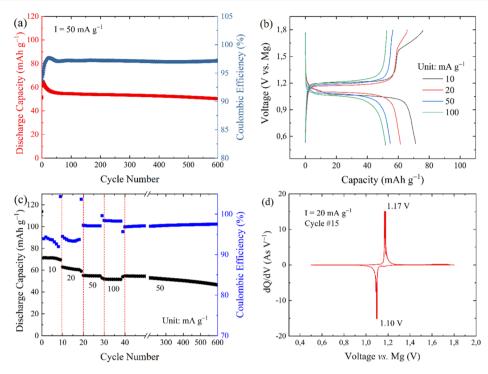
Figure 6. (a) Initial voltage profiles of the cell with the $Mg[B(hfip)_4]_2$/DME-based electrolyte. (b) Voltage profiles of the cell with 5 mM $Mg(BH_4)_2$ in various cycles. (c,d) Cycling performance of the cells and the respective CE. The inset of (c) shows the capacity change upon extended cycling. All cells were tested with a cutoff voltage of 0.5−2.5 V at 50 mA g^{-1}.

Figure 5 displays the XPS detailed spectra in the Mg 2p, F 1s, and O 1s regions of the electrodes after cycling in the electrolyte without or with additives. In the Mg 2p spectra, there are two peaks detected at 49.5 and 51 eV, which correspond to metallic Mg^0 and oxidized Mg^{2+} species (MgO, MgF_2, and so forth), respectively.[30,31] Comparison of the intensities of these two features demonstrates that Mg^{2+} species were dominant on the surface, indicating that MgO and MgF_2 are major components of the SEI. Since bulk MgO and MgF_2 suffer from a high Mg^{2+} migration energy barrier, the interphase layer is likely to have a porous structure that allows Mg transport. A similar chemically inert interphase was also reported elsewhere for reversible Mg[21] and Ca plating.[32,33] Upon sputtering, the peak of metallic Mg^0 gained successively in intensity and became the dominating signal in the Mg 2p region after removal of ∼30 nm of the surface layer. A slight shift of the peak related to the oxidized species can be noted upon sputtering, which is most presumably related to changes in the chemical environment of these species. The presence of MgO and MgF_2 is corroborated by the detection of the corresponding peaks of these species in the O 1s (MgO: ∼530.5 eV) and F 1s (MgF_2: ∼685.5 eV) detailed spectra. Furthermore, for the topmost surface (measurements before sputtering), the detailed spectra in these two regions also reveal the presence of other species such as $-CF_x$ (F 1s peak at ∼690 eV) and $-CO_x$ (O 1s peak at ∼532.5 eV) groups in the SEI layer.[34] These species are most probably coming from side reactions (e.g., decomposition of the electrolyte) along with Mg plating/stripping and/or the electrolyte residues. In addition, B 1s signals were only detected in the spectra of the topmost surface (Figure S6), which could be due to some electrolyte residues rather than the SEI layer itself.

Comparison of the spectra in Figure 5a,b leads to the conclusion that SEI components, such as MgO, MgF_2, and species that contain $-CF_x$ and $-CO_x$ groups, have a notably higher concentration in the surface layer of the Mg anode cycled with the additive-containing electrolyte. This result is consistent with the quantitative analysis (Figure S5) that SEI formation is easier in the presence of $Mg(BH_4)_2$. Correlating it with the Mg plating/stripping data, the XPS results also demonstrate the beneficial effect of $Mg(BH_4)_2$ on building an SEI layer which allows the anode−electrolyte charge transfer and thereby results in a smaller overpotential. Moreover, the SEI layer ensures chemically and electrochemically stable interfaces which promise a long-term cycling stability at the anode side.

2.3. Full-Cell Performance with the $Mg[B(hfip)_4]_2$/ DME-Based Electrolyte. Finally, the additive effect on the full-cell performance was investigated in Mo_6S_8−Mg cells. Compared to the neat electrolyte-based cell, a significant improvement of the initial capacity was found with the additive-containing electrolytes, as shown in the voltage profiles in Figure 6a. After adding 5 mM $Mg(BH_4)_2$, the cell provided a discharge capacity of 96 mA h g^{-1} in the first cycle. In the following charge process, a distinct voltage plateau appeared at 1.25 V, presumably corresponding to Mg deintercalation from the outer-ring sites. The plateau was followed by a charging slope, which could originate from the extraction of Mg from the inner-ring sites.[35] Increasing the additive concentration to 7.5 mM did not improve the redox reactions except for a slight extension of the charge plateau.

Figure 6b shows the voltage profiles of the cell with 5 mM $Mg(BH_4)_2$. Benefiting from fast anode conditioning and SEI formation, the higher discharge capacity in the first cycle ensured sufficient Mg^{2+} ions inserted into the Mo_6S_8 cathode.

Figure 7. Full-cell test with the electrolyte containing 5 mM $Mg(BH_4)_2$ in the voltage range of 0.5−1.8 V: (a) cycling at 50 mA g^{-1}; (b) typical voltage profiles at different current densities; (c) rate capability; and (d) dQ/dV plot of the 15th cycle from the rate capability test.

Although the Mg^{2+} ions that occupied the inner rings of the Mo_6S_8 cages suffered from the kinetic issue,[27] their occupation boosted further Mg^{2+} ion mobility. Therefore, the cell delivered a stable capacity of ∼70 mA h g^{-1} from the second cycle onward (Figure 6c), with a high CE (Figure 6d). In contrast, the activation process with the neat electrolyte (Figure S7) lasts for 20 cycles with a simultaneous increase in the cell capacity to 68 mA h g^{-1} and a gradual decrease in the voltage hysteresis. This is accompanied by a reduction of the CE from >250% to a stable value of ∼97%, due to the slow occupation of the inner-ring site of Mo_6S_8 in the activation cycles. Once the inner-ring sites were fully occupied, the activation process finished. From then on, both the capacity and CE stabilized. It may be noted that the addition of $Mg(BH_4)_2$ did not lead to a notable negative effect on the long-term cycling performance, as evidenced in the inset of Figure 6c. However, the poor chemical stability of $Mg(BH_4)_2$ needs to be considered for its application as an electrolyte additive in full-cell studies.

Nevertheless, it was noticed that the CE of the full-cell measurement with 5 mM $Mg(BH_4)_2$ shows a decrease to 90% during the first 20 cycles by an increase to 97% after 50 cycles (see Figure S8). The fluctuation of CE could be due to the decomposition of BH_4^- at high voltages, which could be suppressed by narrowing the cutoff range. In fact, by lowering the upper cutoff voltage to 1.8 V, a cell with the same configuration provides a higher CE of >94% for the initial 50 cycles. As shown in Figure 7a, it also exhibits a stable discharge capacity of ∼50 mA h g^{-1} at a current density of 50 mA g^{-1} for up to 600 cycles, demonstrating a superior cycling stability. Higher capacities of 71 and 61 mA h g^{-1} were obtained at lower current rates of 10 and 20 mA g^{-1}, respectively (Figure 7b). Meanwhile, the discharge plateau at 1.2 V only appears at low current density, confirming the kinetics issue for Mg storage at the Mo_6S_8 inner rings. For comparison, ion mobility

in the outer rings is high enough even for a dis-/charge at a high current of 100 mA g^{-1} (∼0.8 C), and the cell delivers a capacity of 52 mA h g^{-1}. Good capacity retention shown in Figure 7c indicates an excellent rate capability. In addition, the cell shows a low voltage hysteresis. In the dQ/dV plot (Figure 7d), the overpotential for de-/magnesiation was only 0.07 V at 20 mA g^{-1}, indicating a high energy efficiency.

■ CONCLUSIONS

In summary, we have demonstrated a reversible Mg intercalation into Chevrel phase Mo_6S_8 from the noncorrosive electrolyte $Mg[B(hfip)_4]_2$/DME. To reach stable and reversible Mg storage, the respective cell requires activation cycles, during which a stable anode−electrolyte interface was established. It was found that BH_4^- can boost the activation process by efficiently removing the native oxide layer on the Mg surface and promoting the SEI formation. With only 5 mM $Mg(BH_4)_2$ additive to the $Mg[B(hfip)_4]_2$/DME electrolyte, a lower charge transfer resistance and reduced overpotentials in the first cycles can be achieved. The improvement at the anode side in turn helps initial Mg^{2+} insertion into the Mo_6S_8 cathode, resulting in a conditioning-free charge−discharge process. By combining the Mo_6S_8 cathode and the additive-containing electrolyte, the cell exhibits an excellent cycling stability for up to 600 cycles with a superior rate capability and a low voltage hysteresis. The current study points out the significant role of the electrode−electrolyte interfaces in the Mg-based chemistry. It also highlights the facile strategy by applying functional additives for further optimizing the simple-salt electrolyte systems.

■ ASSOCIATED CONTENT

ⓢ Supporting Information

The Supporting Information is available free of charge at https://pubs.acs.org/doi/10.1021/acsami.1c08476.

Materials and methods, additional electrochemical data, XPS B 1s spectra, and elemental content determined by XPS (PDF)

AUTHOR INFORMATION

Corresponding Authors

Zhenyou Li − *Helmholtz Institute Ulm (HIU) Electrochemical Energy Storage, D-89081 Ulm, Germany;* ⊙ orcid.org/0000-0001-9624-2124; Email: zhenyou.li@kit.edu

Zhirong Zhao-Karger − *Helmholtz Institute Ulm (HIU) Electrochemical Energy Storage, D-89081 Ulm, Germany; Institute of Nanotechnology (INT), Karlsruhe Institute of Technology (KIT), D-76021 Karlsruhe, Germany;* ⊙ orcid.org/0000-0002-7233-9818; Email: zhirong.zhao-karger@kit.edu

Authors

Thomas Diemant − *Helmholtz Institute Ulm (HIU) Electrochemical Energy Storage, D-89081 Ulm, Germany*

Zhen Meng − *Helmholtz Institute Ulm (HIU) Electrochemical Energy Storage, D-89081 Ulm, Germany;* ⊙ orcid.org/0000-0001-5756-9159

Yanlei Xiu − *Helmholtz Institute Ulm (HIU) Electrochemical Energy Storage, D-89081 Ulm, Germany*

Adam Reupert − *Helmholtz Institute Ulm (HIU) Electrochemical Energy Storage, D-89081 Ulm, Germany*

Liping Wang − *Helmholtz Institute Ulm (HIU) Electrochemical Energy Storage, D-89081 Ulm, Germany;* ⊙ orcid.org/0000-0002-4113-2208

Maximilian Fichtner − *Helmholtz Institute Ulm (HIU) Electrochemical Energy Storage, D-89081 Ulm, Germany; Institute of Nanotechnology (INT), Karlsruhe Institute of Technology (KIT), D-76021 Karlsruhe, Germany*

Complete contact information is available at:
https://pubs.acs.org/10.1021/acsami.1c08476

Author Contributions

The manuscript was written with contributions of all authors. All authors have given approval to the final version of the manuscript.

Notes

The authors declare no competing financial interest.

All experimental data that support the findings of this study are readily available upon reasonable request from the corresponding authors.

REFERENCES

(1) Jäckle, M.; Helmbrecht, K.; Smits, M.; Stottmeister, D.; Groß, A. Self-diffusion barriers: possible descriptors for dendrite growth in batteries? *Energy Environ. Sci.* **2018**, *11*, 3400−3407.

(2) Canepa, P.; Sai Gautam, G.; Hannah, D. C.; Malik, R.; Liu, M.; Gallagher, K. G.; Persson, K. A.; Ceder, G. Odyssey of Multivalent Cathode Materials: Open Questions and Future Challenges. *Chem. Rev.* **2017**, *117*, 4287−4341.

(3) Aurbach, D.; Lu, Z.; Schechter, A.; Gofer, Y.; Gizbar, H.; Turgeman, R.; Cohen, Y.; Moshkovich, M.; Levi, E. Prototype systems for rechargeable magnesium batteries. *Nature* **2000**, *407*, 724−727.

(4) Muldoon, J.; Bucur, C. B.; Gregory, T. Quest for Nonaqueous Multivalent Secondary Batteries: Magnesium and Beyond. *Chem. Rev.* **2014**, *114*, 11683−11720.

(5) Mohtadi, R.; Mizuno, F. Magnesium batteries: Current state of the art, issues and future perspectives. *Beilstein J. Nanotechnol.* **2014**, *5*, 1291−1311.

(6) Gregory, T. D.; Hoffman, R. J.; Winterton, R. C. Nonaqueous Electrochemistry of Magnesium: Applications to Energy Storage. *J. Electrochem. Soc.* **1990**, *137*, 775−780.

(7) Rajput, N. N.; Seguin, T. J.; Wood, B. M.; Qu, X.; Persson, K. A. Elucidating Solvation Structures for Rational Design of Multivalent Electrolytes—A Review. *Top. Curr. Chem.* **2018**, *376*, 19.

(8) Yu, Y.; Baskin, A.; Valero-Vidal, C.; Hahn, N. T.; Liu, Q.; Zavadil, K. R.; Eichhorn, B. W.; Prendergast, D.; Crumlin, E. J. Instability at the Electrode/Electrolyte Interface Induced by Hard Cation Chelation and Nucleophilic Attack. *Chem. Mater.* **2017**, *29*, 8504−8512.

(9) Mohtadi, R.; Tutusaus, O.; Arthur, T. S.; Zhao-Karger, Z.; Fichtner, M. The metamorphosis of rechargeable magnesium batteries. *Joule* **2021**, *5*, 581−617.

(10) Connell, J. G.; Zorko, M.; Agarwal, G.; Yang, M.; Liao, C.; Assary, R. S.; Strmcnik, D.; Markovic, N. M. Anion Association Strength as a Unifying Descriptor for the Reversibility of Divalent Metal Deposition in Nonaqueous Electrolytes. *ACS Appl. Mater. Interfaces* **2020**, *12*, 36137−36147.

(11) He, S.; Nielson, K. V.; Luo, J.; Liu, T. L. Recent advances on MgCl2 based electrolytes for rechargeable Mg batteries. *Energy Storage Mater.* **2017**, *8*, 184−188.

(12) Tutusaus, O.; Mohtadi, R.; Arthur, T. S.; Mizuno, F.; Nelson, E. G.; Sevryugina, Y. V. An Efficient Halogen-Free Electrolyte for Use in Rechargeable Magnesium Batteries. *Angew. Chem., Int. Ed.* **2015**, *54*, 7900−7904.

(13) Attias, R.; Salama, M.; Hirsch, B.; Goffer, Y.; Aurbach, D. Anode-Electrolyte Interfaces in Secondary Magnesium Batteries. *Joule* **2019**, *3*, 27−52.

(14) Kim, S. S.; See, K. A. Activating Magnesium Electrolytes through Chemical Generation of Free Chloride and Removal of Trace Water. *ACS Appl. Mater. Interfaces* **2021**, *13*, 671−680.

(15) Zhao-Karger, Z.; Gil Bardaji, M. E.; Fuhr, O.; Fichtner, M. A new class of non-corrosive, highly efficient electrolytes for rechargeable magnesium batteries. *J. Mater. Chem. A* **2017**, *5*, 10815−10820.

(16) Zhang, Z.; Cui, Z.; Qiao, L.; Guan, J.; Xu, H.; Wang, X.; Hu, P.; Du, H.; Li, S.; Zhou, X.; Dong, S.; Liu, Z.; Cui, G.; Chen, L. Novel Design Concepts of Efficient Mg-Ion Electrolytes toward High-Performance Magnesium−Selenium and Magnesium−Sulfur Batteries. *Adv. Energy Mater.* **2017**, *7*, 1602055.

(17) Luo, J.; Bi, Y.; Zhang, L.; Zhang, X.; Liu, T. L. A Stable, Non-Corrosive Perfluorinated Pinacolatoborate Mg Electrolyte for Rechargeable Mg Batteries. *Angew. Chem., Int. Ed.* **2019**, *58*, 6967−6971.

(18) Tutusaus, O.; Mohtadi, R.; Singh, N.; Arthur, T. S.; Mizuno, F. Study of Electrochemical Phenomena Observed at the Mg Metal/Electrolyte Interface. *ACS Energy Lett.* **2017**, *2*, 224−229.

(19) Zhao-Karger, Z.; Liu, R.; Dai, W.; Li, Z.; Diemant, T.; Vinayan, B. P.; Bonatto Minella, C.; Yu, X.; Manthiram, A.; Behm, R. J.; Ruben, M.; Fichtner, M. Toward Highly Reversible Magnesium−Sulfur

Batteries with Efficient and Practical Mg[B(hfip)4]2 Electrolyte. *ACS Energy Lett.* **2018**, 3, 2005−2013.

(20) Meng, Z.; Foix, D.; Brun, N.; Dedryvère, R.; Stievano, L.; Morcrette, M.; Berthelot, R. Alloys to Replace Mg Anodes in Efficient and Practical Mg-Ion/Sulfur Batteries. *ACS Energy Lett.* **2019**, 4, 2040−2044.

(21) Li, B.; Masse, R.; Liu, C.; Hu, Y.; Li, W.; Zhang, G.; Cao, G. Kinetic surface control for improved magnesium-electrolyte interfaces for magnesium ion batteries. *Energy Storage Mater.* **2019**, 22, 96−104.

(22) Lv, R.; Guan, X.; Zhang, J.; Xia, Y.; Luo, J. Enabling Mg metal anodes rechargeable in conventional electrolytes by fast ionic transport interphase. *Natl. Sci. Rev.* **2020**, 7, 333−341.

(23) Sa, N.; Pan, B.; Saha-Shah, A.; Hubaud, A. A.; Vaughey, J. T.; Baker, L. A.; Liao, C.; Burrell, A. K. Role of Chloride for a Simple, Non-Grignard Mg Electrolyte in Ether-Based Solvents. *ACS Appl. Mater. Interfaces* **2016**, 8, 16002−16008.

(24) Li, Z.; Vinayan, B. P.; Jankowski, P.; Njel, C.; Roy, A.; Vegge, T.; Maibach, J.; Lastra, J. M. G.; Fichtner, M.; Zhao-Karger, Z. Multi-Electron Reactions Enabled by Anion-Based Redox Chemistry for High-Energy Multivalent Rechargeable Batteries. *Angew. Chem., Int. Ed.* **2020**, 59, 11483−11490.

(25) Li, Z.; Mu, X.; Zhao-Karger, Z.; Diemant, T.; Behm, R. J.; Kübel, C.; Fichtner, M. Fast kinetics of multivalent intercalation chemistry enabled by solvated magnesium-ions into self-established metallic layered materials. *Nat. Commun.* **2018**, 9, 5115.

(26) Levi, E.; Gershinsky, G.; Aurbach, D.; Isnard, O.; Ceder, G. New Insight on the Unusually High Ionic Mobility in Chevrel Phases. *Chem. Mater.* **2009**, 21, 1390−1399.

(27) Levi, E.; Lancry, E.; Mitelman, A.; Aurbach, D.; Ceder, G.; Morgan, D.; Isnard, O. Phase Diagram of Mg Insertion into Chevrel Phases, MgxMo6T8 (T = S, Se). 1. Crystal Structure of the Sulfides. *Chem. Mater.* **2006**, 18, 5492−5503.

(28) Mohtadi, R.; Matsui, M.; Arthur, T. S.; Hwang, S.-J. Magnesium Borohydride: From Hydrogen Storage to Magnesium Battery. *Angew. Chem., Int. Ed.* **2012**, 51, 9780−9783.

(29) Wang, X.; Yasukawa, E.; Mori, S. Inhibition of anodic corrosion of aluminum cathode current collector on recharging in lithium imide electrolytes. *Electrochim. Acta* **2000**, 45, 2677−2684.

(30) Yoo, H. D.; Han, S.-D.; Bolotin, I. L.; Nolis, G. M.; Bayliss, R. D.; Burrell, A. K.; Vaughey, J. T.; Cabana, J. Degradation Mechanisms of Magnesium Metal Anodes in Electrolytes Based on (CF3SO2)2N− at High Current Densities. *Langmuir* **2017**, 33, 9398−9406.

(31) Kang, S.-J.; Kim, H.; Hwang, S.; Jo, M.; Jang, M.; Park, C.; Hong, S.-T.; Lee, H. Electrolyte Additive Enabling Conditioning-Free Electrolytes for Magnesium Batteries. *ACS Appl. Mater. Interfaces* **2019**, 11, 517−524.

(32) Wang, D.; Gao, X.; Chen, Y.; Jin, L.; Kuss, C.; Bruce, P. G. Plating and stripping calcium in an organic electrolyte. *Nat. Mater.* **2018**, 17, 16−20.

(33) Li, Z.; Fuhr, O.; Fichtner, M.; Zhao-Karger, Z. Towards stable and efficient electrolytes for room-temperature rechargeable calcium batteries. *Energy Environ. Sci.* **2019**, 12, 3496−3501.

(34) Bhaghavathi Parambath, V.; Zhao-Karger, Z.; Diemant, T.; Jäckle, M.; Li, Z.; Scherer, T.; Gross, A.; Behm, R. J.; Fichtner, M. Investigation on the formation of Mg metal anode/electrolyte interfaces in Mg/S batteries with electrolyte additives. *J. Mater. Chem. A* **2020**, 8, 22998−23010.

(35) Richard, J.; Benayad, A.; Colin, J.-F.; Martinet, S. Charge Transfer Mechanism into the Chevrel Phase Mo6S8 during Mg Intercalation. *J. Phys. Chem. C* **2017**, 121, 17096−17103.